Design and fabrication of microcoil metamaterial absorber for the sub-terahertz region

VERDAD C. AGULTO,[1] ZIQI LING,[1] ZIXI ZHAO,[1] SHIYU FENG,[1] KOSAKU KATO,[1] MOTOHARU HAGA,[2] VALYNN KATRINE MAG-USARA,[1] MASASHI YOSHIMURA,[1] MAKOTO NAKAJIMA[1,*]

[1]*Institute of Laser Engineering, Osaka University, 2-6 Yamadaoka, Suita, Osaka 565-0871, Japan*
[2]*Daicel Corporation, 3-1 Ofuka-cho, Kita-ku, Osaka 530-0011, Japan*
nakajima.makoto.ile@osaka-u.ac.jp

Received XX Month XXXX; revised XX Month, XXXX; accepted XX Month XXXX; posted XX Month XXXX (Doc. ID XXXXX); published XX Month XXXX

The development of electromagnetic wave absorbers operating in the sub-terahertz (sub-THz) region is necessary in 6G communications. We designed and fabricated a sub-THz metamaterial absorber based on metal microcoils embedded and periodically arranged in a dielectric substrate. The microcoil parameters were optimized by calculating the electromagnetic response of the metamaterial using finite element analysis. An actual metamaterial was then fabricated based on the optimized parameters and characterized using THz time-domain spectroscopy. Our microcoil absorber exhibits an absorptance of > 80 % and a high shielding performance at about 250 GHz. The resonance frequency can be precisely adjusted by modifying the microcoil array dimensions.

The future of 6G communications lies in the sub-terahertz (sub-THz) band, i.e., the frequency spectrum between 90–300 GHz. Although the deployment of 5G technology is still underway, researchers are already exploring beyond the 5G region. This range of frequencies is expected to be utilized for ultra-high speed wireless communications enabling very high data rate and enormous bandwidth that is several tens of GHz [1]. Owing to the significant progress of THz technology, a wide array of THz functional devices and diagnostic applications have been made possible [2–7]. For the advancement of telecommunications utilizing THz waves, there is a need for the development of appropriate electromagnetic interference (EMI) shielding materials that must protect the communication systems from disruptive external sources of electromagnetic signals. EMI shielding pertains to the attenuation of the propagating electromagnetic waves by reflection and/or absorption [8]. Reflected electromagnetic waves, however, cause secondary electromagnetic pollution which can adversely affect the normal operation of equipment and devices. Thus, absorption-dominant shielding materials are more desirable in enhancing the isolation among devices and in reducing EMI. Absorbers with operating frequency at the sub-THz region are thereby necessary for EMI shielding application in future wireless communications. For this purpose, magnetic materials with resonance absorption peaks within 100–200 GHz have been proposed as an electromagnetic wave absorber [9].

Metamaterial absorbers are notable for their tunable absorption properties that depend on the structural parameters of the metamaterial. Metamaterials are artificially engineered sub-wavelength structures (meta-atoms) that can actively manipulate electromagnetic waves based on their geometric design. By changing the size, shape, and distribution of the meta-atoms, the electromagnetic response of the metamaterial to incident radiation can be tailored. Various metamaterial geometries based on two- and three-dimensional (2D, 3D) structures have been demonstrated catering to different applications. Planar 2D metamaterials are favorable for device integration because they are ultrathin; however, it is challenging to obtain a large bandwidth with a very small absorber thickness. As a workaround, planar metamaterials can be stacked together to produce multi-layered 3D absorbers with enhanced absorption and bandwidth [10].

Helical metamaterials are interesting 3D structures because an individual helix supports many internal resonances [11,12]. They are commonly employed as circular polarizers owing to their circular dichroism [11,13–15], whereby a helical structure selectively interacts with light whose polarization is the same direction as the handedness of the helix. Furthermore, it has been reported that bio-templated metal microcoils with electromagnetic responses in the THz region show remarkable transmission loss and very low reflectance, indicating high absorption of THz waves [16]. Thus, helical metamaterials based on metal microcoils have potential for absorber applications, and their operation frequency can be designed in the sub-THz band depending on the parameters of the microcoils. For the characterization of such metamaterial devices, THz spectroscopy is a necessary tool which has been widely implemented in elucidating the properties of various functional materials [17–19].

Metal microcoils offer a cost-effective alternative to intricate 3D metamaterials produced through advanced microfabrication techniques. Metal coils are industrially manufactured as commonplace components such as springs and inductors within various mechanical and electronic devices. Remarkably, micrometer-scale coils are currently mass-produced using mechanical winding techniques, making them readily available in commercial markets. Despite their accessibility, these mechanically made microcoils remain largely underexplored as sub-THz wave absorbers. In this study, we then investigated and developed a metal microcoil array as an electromagnetic wave absorber for the sub-THz region. The incident waves were linearly polarized, and normal incidence was considered. We utilized tungsten and polyester as the materials for the microcoil and the substrate where the microcoils were embedded, respectively. First, we designed the metamaterial and simulated its electromagnetic response for different microcoil parameters. We selected the design with the best parameters for an absorber and fabricated an actual metamaterial sample. Then, we used THz time-domain spectroscopy to characterize the actual sample and compared the experimental results with the simulations.

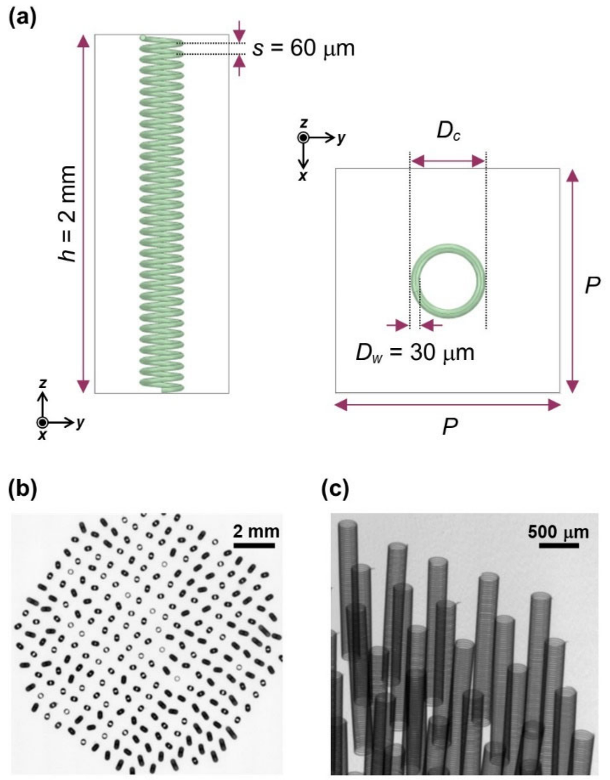

Fig. 1. Microcoil metamaterial: (a) model of the unit cell and (b, c) x-ray images of an actual sample taken from the top and at a tilted angle.

The parameters of the microcoil unit cell are defined in Fig. 1(a). The coil is characterized by the coil diameter D_c, the wire diameter D_w = 30 μm, the pitch or spacing between the turns s = 60 μm, and the height h = 2 mm. The coils, which are made of tungsten, are embedded in a polyester substrate with the same height and are periodically arranged in a square lattice by a period P. We performed numerical calculations of the electromagnetic response using a commercial finite element analysis software, Ansys HFSS. The scattering parameters were calculated using realistic permittivity and dielectric loss values of tungsten and the polyester substrate. The permittivity of tungsten was derived based on the Drude model where the plasma frequency $\omega_p = 5.17 \times 10^4$ cm^{-1} and the scattering time $\omega_\tau = 4.87 \times 10^2$ cm^{-1} [20]. On the other hand, the permittivity of the polyester substrate was obtained experimentally through THz-TDS. Furthermore, the propagation (polarization) direction of the incident THz radiation is parallel (perpendicular) to the helical axis z. Periodic boundary conditions were applied along the x and y directions.

We varied the coil diameter and the period of the array to find the optimal parameters for our desired absorber. Figure 2(a) shows the calculated transmittance spectra of metal microcoil metamaterials with different coil diameters D_c = 250, 300, 350 μm, referred to as D250, D300, and D350, respectively. Here the period was fixed at P = 750 μm. Figure 2(b) shows the calculated transmittance spectra for different periods P = 500, 750, 1000 μm and a fixed coil diameter D_c = 250 μm. The other parameters are fixed to their respective values in Fig. 1(a). The transmittance is expressed in decibel (dB) so that the characteristic resonances are discernible. The broad resonance band is attributed to the combination of internal resonances and their mutual coupling in each coil and the coupling between adjacent coil resonators [11–13]. In Fig. 2(a), the resonance band shifts to lower frequencies as D_c is increased. Our microcoil resonator is operating in the axial mode of a helical antenna. The axial mode dominates when the circumference of the helix is proportional to the wavelength and the electromagnetic wave propagates along the helix axis [21]. A bigger circumference leads to a longer resonance wavelength, thus the resonance frequency redshifts with increasing coil diameter. In Fig. 2(b), the resonance band narrows as the period is increased. This is attributed to the weaker lateral interaction between adjacent coils as their spacing widens [22]. Furthermore, the depth of the resonance band becomes shallower with decreasing D_c and increasing P. This is because decreasing the size of the coils or increasing their spacing dilutes the array, thereby weakening the resonance strength.

In Fig. 2, the transmittance minimum in each spectrum is indicated by a vertical dashed line. The calculated transmittance (T), reflectance (R), and absorptance (A) values at this resonance frequency for different coil diameters at a fixed period and for different periods at a fixed coil diameter are summarized in Table 1 and Table 2, respectively. Note that these values follow the relation $A = 1 - T - R$. For absorber applications, high absorption (A > 80 %) and high shielding performance are desired. The shielding effectiveness (SE) is defined by [8]

$$SE = 10 \log \left| \frac{1}{T} \right|. \quad (1)$$

To achieve a power loss of > 99 % after shielding, a value of SE > 20 dB is required (i.e., T < – 20 dB). We used these criteria to select the best parameters for our metamaterial absorber. Based on the simulation results, the criteria of A > 80 % and T < – 20 dB at the resonance frequency are met when D_c = 250 μm and P = 750 μm. Hence, we fabricated a sample using these microcoil parameters with the rest of the parameters fixed to the respective values in Fig. 1(a).

To fabricate the metamaterial sample, commercial tungsten coils were individually inserted into the holes of a stainless-steel plate that was used as a guide to periodically arrange the coils. The coils were produced by a filament winding process. Note that the coils had the same handedness and that each helix had random starting points. The coil array was then embedded in a polyester resin, and the stainless-steel plate was removed. Grinding was carried out on the top and bottom sides of the sample to achieve a thickness of (2.0 ± 0.1) mm. The x-ray images of the coil array are shown in Figs. 1(b) and 1(c). We employed transmission and reflection THz-TDS measurements to characterize the optical properties of the sample. The THz-TDS system (Advantest TAS7500TS) utilized two oscillatory frequency synchronous type fiber lasers (λ = 1.55 μm, pulse width ≤ 50 fs, pulse repetition rate = 50 MHz) and fiber-pigtailed photoconductive antennas for THz generation and THz detection. The sampling of the THz field was based on an electronically controlled sweep method. We used an aperture that was slightly smaller than the microcoil array and had a diameter of 10 mm. The experimental results were then compared to the simulations.

Figure 3 shows the transmittance spectrum of the sample measured by THz-TDS together with the calculated spectrum for comparison. The overall shapes of the experimental and the calculated transmittance spectra are consistent. The transmittance minimum of the sample is found at 252 GHz where T = – 27 dB. At this frequency, the measured reflectance of the sample is 10.5 %, resulting in an experimental absorptance of 89.3 %. The experimental results have excellent agreement with the simulations. The high attenuation of THz waves can be mainly attributed to ohmic and radiative losses in the metallic microcoils [23].

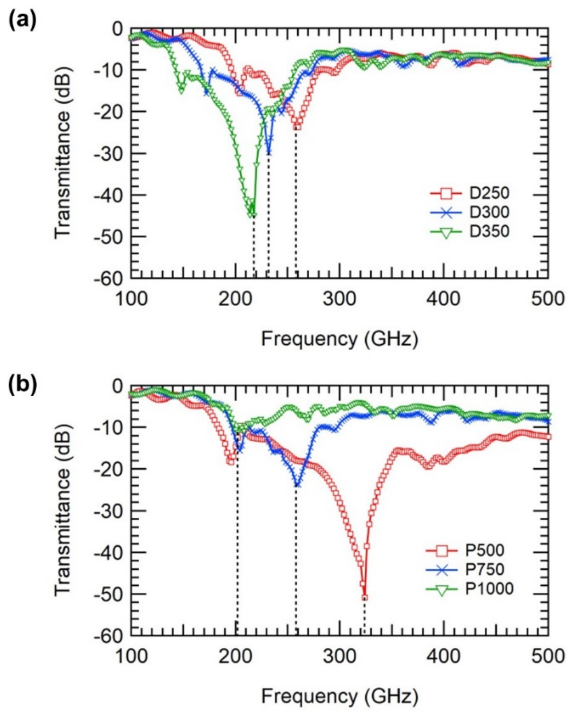

Fig. 2. Calculated transmittance spectra of the microcoil metamaterial: (a) for different D_c = 250, 300, 350 μm at fixed P = 250 μm; (b) for different P = 500, 750, 1000 μm at fixed D_c = 250 μm.

Table 1. Resonance Properties for D_c = 250, 300, 350 μm at Fixed P = 750 μm

	f (GHz)	T (dB)	T (%)	R (%)	A (%)
D250	258	– 23.7	0.430	17.2	82.4
D300	232	– 29.8	0.00104	28.6	71.3
D350	218	– 44.8	0.0000328	56.3	43.7

Table 2. Resonance Properties for P = 500, 750, 1000 μm at Fixed D_c = 250 μm

	f (GHz)	T (dB)	T (%)	R (%)	A (%)
P500	324	– 50.8	0.000830	37.6	62.4
P750	258	– 23.7	0.430	17.2	82.4
P1000	202	– 11.1	13.8	7.78	78.4

For a helical metamaterial such as the microcoils, the electromagnetic response can be described by the antenna theory [21]. Helical antennas have two modes of operation: the normal mode and the axial mode. In the normal mode, the dimensions of the helix are small compared to the wavelength of operation and the radiation field is normal to the helical axis. In the axial mode, the circumference of the helix is proportional to the wavelength and the electromagnetic wave travels along the helical axis. Provided that the wire is thin ($D_w << D_c$) and that at least 3 helix pitches are used, the resonance frequency f of a helical antenna in an axial mode of operation is in the interval [12,15,21]

$$\frac{1}{n}\frac{3c_0}{4\pi D_c} < f < \frac{1}{n}\frac{4c_0}{3\pi D_c} \tag{2}$$

where c_0 is the speed of light in free space and n is the refractive index of the material where the coils are embedded. Our helical metamaterial operates in the axial mode. Given D_c = 250 μm and n ≈ 1.7 for polyester in the frequency region of interest, the estimated resonance frequency is expected between 170 and 300 GHz, which is similar with the observed resonance band in our experiment and simulation.

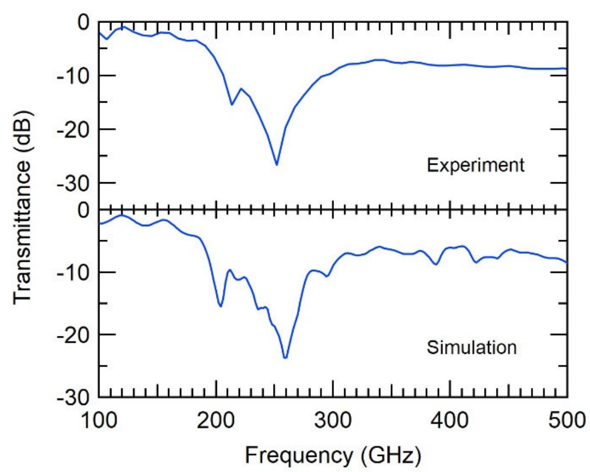

Fig. 3. Experimental and calculated THz transmittance spectra of metal microcoils (D_c = 250 μm) embedded in polyester and arranged in a square lattice (P = 750 μm).

Following the helical antenna theory, the frequency of operation is strongly dependent on the diameter of the helix. The resonance frequency is also influenced by the period due to lateral interaction effects between adjacent helices. Thus, by modifying the coil array parameters, the resonance frequency of the metamaterial can be adjusted according to specific requirements. Figure 4(a) shows how the resonance frequency, which corresponds to the transmittance minimum, varies with coil diameter and period. The corresponding absorptance at each resonance frequency is also shown in Fig. 4(b). The results are obtained by calculating the electromagnetic responses for D_c = 250–400 μm and P = 600–750 μm with a respective step of 50 μm while the rest of the parameters are fixed to their respective values in Fig. 1(a). Note that the data points used to generate the 3D surface plots lie on the intersection points of the gridlines and major axes and that the color scales represent the frequency and absorptance values (see Tables S1 to S4 in Supplement 1 for underlying values). In general, we observe a redshift of the resonance frequency with increasing coil diameter and period. Furthermore, given a fixed period the absorptance generally increases as the coil diameter is decreased from 400 to 250 μm. For these sets of parameters, the shielding performance is generally above 20 dB, i.e., $T < -20$ dB (see Supplement 1). However, when the coils have a wide diameter and/or packed closely to one another, there is high reflection loss thereby resulting in weak absorption. Therefore, the resonance frequency of the microcoil array metamaterial can be easily adjusted by modifying the microcoil parameters such as coil diameter and period, but the absorption properties are sensitive to the combination of such parameters.

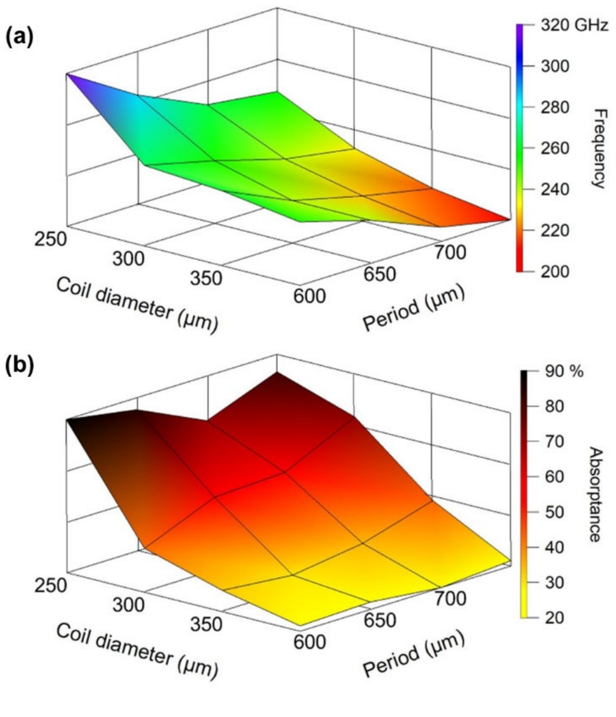

Fig. 4. (a) Effect of the coil diameter and the period on the resonance frequency and (b) the corresponding absorptance of the microcoil metamaterial based on simulations. See **Supplement 1** for underlying values. (Color version available online)

In summary, we designed and fabricated a helical metamaterial based on metal microcoils embedded in a dielectric substrate. Our metamaterial exhibits high absorption (A > 80 %) and high shielding performance (SE > 20 dB) at about 250 GHz, with a resonance band in the 170–300 GHz region. With these properties, our metamaterial has a potential application as a shield of wireless high-frequency modules to improve the electromagnetic compatibility of future 6G devices. By changing the structural parameters of the microcoil such as the coil diameter and the period of the array, the resonance frequency of the metamaterial can be adjusted in the sub-THz region and the absorption properties can be optimized. Furthermore, the metal microcoils used in our study can be easily mass-produced through an industrial process, and their parameters can be conveniently controlled without any complicated templating method, making them a practical unit of metamaterial absorbers and devices.

Funding. This work was supported by JSPS KAKENHI Grant Numbers JP23K17748 and JP20H02206.

Disclosures. The authors declare no conflicts of interest.

Data availability. Data underlying the results presented in this paper are not publicly available at this time but may be obtained from the authors upon reasonable request.

Supplemental document. See Supplement 1 for supporting content.

References

1. S. Tripathi, N. v. Sabu, A. K. Gupta, *et al*., *6G Mobile Wireless Networks* (2021), pp. 83–121.
2. A. Iba, C. W. Domier, M. Ikeda, *et al*., Opt. Lett. **46**, 4912 (2021).
3. L. Wang, R.Xiao, S. Yang, *et al*., Opt. Lett. **45**, 5892 (2020).
4. D. Li, M. Nakajima, M. Tani, *et al*., Sci. Rep. **9**, 6804 (2019).
5. L. Wang, S. Ge, W. Hu, *et al*., Opt. Express **25**, 23873 (2017).
6. K. Kato, K. Takano, Y. Tadokoro, *et al*., Opt. Lett. **41**, 2125 (2016).
7. M. Ota, K. Kan, S. Komada, *et al*., Nat. Phys. **18**, 1436 (2022).
8. M. Peng and F. Qin, J. Appl. Phys. **130**, 225108 (2021).
9. A. Namai, S. Sakurai, M. Nakajima, *et al*., J. Am. Chem. Soc. **131**, 1170 (2009).
10. A. Choudhary, S. Pal, and G. Sarkhel, Int. J. Microw. Wirel. Technol. **15**, 347 (2023).
11. J. K. Gansel, M. Thiel, M. S. Rill, *et al*., Science **325**, 1513 (2009).
12. J. K. Gansel, M. Wegener, S. Burger, *et al*., Opt. Express **18**, 1059 (2010).
13. S. Li, Z. Yang, J. Wang, *et al*., J. Opt. Soc. Am. A **28**, 19 (2011).
14. Y. Yu, Z. Yang, M. Zhao, *et al*., J. Opt. **13**, 055104 (2011).
15. H. Tomita, K. Hashimoto, K. Takeya, *et al*., Opt. Lett. **46**, 2232 (2021).
16. K. Kamata, Z. Piao, S. Suzuki, *et al*., S. Horaguchi, A. Belay, T. Tanaka, K. Takano, and M. Hangyo, Sci. Rep. **4**, 4919 (2015).
17. V. C. Agulto, K. Toya, T. N. K. Phan, *et al*., Appl. Phys. Lett. **118**, 042101 (2021).
18. V. C. Agulto, T. Iwamoto, H. Kitahara, *et al*., Sci. Rep. **11**, 18129 (2021).
19. G. Fitzky, M. Nakajima, Y. Koike, *et al*., Phys. Rev. Lett. **127**, 107401 (2021).
20. M. A. Ordal, R. J. Bell, R. W. Alexander, *et al*., Appl. Opt. **24**, 4493 (1985).
21. J. D. Kraus, "The Helical Antenna," in *Antennas*, 2nd ed. (McGraw-Hill, 1997), pp. 265–339.
22. Z. He, L. Wu, Y. Liu, *et al*., J. Appl. Phys. **127**, 174901 (2020).
23. T. Notake, T. Iyoda, T. Arikawa, *et al*., Sci. Rep. **11**, 3310 (2021).

References

1. S. Tripathi, N. v. Sabu, A. K. Gupta, and H. S. Dhillon, "Millimeter-Wave and Terahertz Spectrum for 6G Wireless," in *6G Mobile Wireless Networks* (2021), pp. 83–121.
2. A. Iba, C. W. Domier, M. Ikeda, A. Mase, M. Nakajima, A.-V. Pham, and N. C. Luhmann, "Subdiffraction focusing with a long focal length using a terahertz-wave super-oscillatory lens," Optics Letters **46**, 4912 (2021).
3. L. Wang, R.Xiao, S. Yang, H. Qiu, Z. Shen, P. Lv, C. Zhang, W. Wei, M. Nakajima, B. Jin, and Y. Q. Lu, "3D porous graphene-assisted capsulized cholesteric liquid crystals for terahertz power visualization," Optics Letters **45**, 5892 (2020).
4. D. Li, M. Nakajima, M. Tani, J. Yang, H. Kitahara, M. Hashida, M. Asakawa, W. Liu, Y. Wei, and Z. Yang, "Terahertz Radiation from Combined Metallic Slit Arrays" Scientific Reports **9**, 6804 (2019).
5. L. Wang, S. Ge, W. Hu, M. Nakajima, and Y. Lu, "Graphene-assisted high-efficiency liquid crystal tunable terahertz metamaterial absorber," Optics Express **25**, 23873 (2017).
6. K. Kato, K. Takano, Y. Tadokoro, and M. Nakajima, "Graphene-assisted high-efficiency liquid crystal tunable terahertz metamaterial absorber," Optics Letters **41**, 2125 (2016).
7. M. Ota, K. Kan, S. Komada, Y. Wang, V. Agulto, V. K. Mag-usara, Y. Arikawa, M. Asakawa, Y. Sakawa, T. Matsui, and M. Nakajima, "Ultrafast visualization of an electric field under the Lorentz transformation," Nature Physics **18**, 1436 (2022).
8. M. Peng and F. Qin, "Clarification of basic concepts for electromagnetic interference shielding effectiveness," Journal of Applied Physics **130**, 225108 (2021).
9. A. Namai, S. Sakurai, M. Nakajima, T. Suemoto, K. Matsumoto, M. Goto, S. Sasaki, and S. Ohkoshi, "Synthesis of an Electromagnetic Wave Absorber for High-Speed Wireless Communication," Journal of the American Chemical Society **131**, 1170 (2009).
10. A. Choudhary, S. Pal, and G. Sarkhel, "Broadband millimeter-wave absorbers: a review," International Journal of Microwave and Wireless Technologies **15**, 347 (2023).
11. J. K. Gansel, M. Thiel, M. S. Rill, M. Decker, K. Bade, V. Saile, G. von Freymann, S. Linden, and M. Wegener, "Gold Helix Photonic Metamaterial as Broadband Circular Polarizer," Science **325**, 1513 (2009).
12. J. K. Gansel, M. Wegener, S. Burger, and S. Linden, "Gold helix photonic metamaterials: A numerical parameter study," Optics Express **18**, 1059 (2010).
13. S. Li, Z. Yang, J. Wang, and M. Zhao, "Broadband terahertz circular polarizers with single- and double-helical array metamaterials," Journal of the Optical Society of America A **28**, 19 (2011).
14. Y. Yu, Z. Yang, M. Zhao, and P. Lu, "Broadband optical circular polarizers in the terahertz region using helical metamaterials," Journal of Optics **13**, 055104 (2011).
15. H. Tomita, K. Hashimoto, K. Takeya, and S. R. Tripathi, "Development of a terahertz wave circular polarizer using a 2D array of metallic helix metamaterial," Optics Letters **46**, 2232 (2021).
16. K. Kamata, Z. Piao, S. Suzuki, T. Fujimori, W. Tajiri, K. Nagai, T. Iyoda, A. Yamada, T. Hayakawa, M. Ishiwara, S. Horaguchi, A. Belay, T. Tanaka, K. Takano, and M. Hangyo, "Spirulina-Templated Metal Microcoils with Controlled Helical Structures for THz Electromagnetic Responses," Scientific Reports **4**, 4919 (2015).
17. V. C. Agulto, K. Toya, T. N. K. Phan, V. K. Mag-usara, J. Li, M. J. F. Empizo, T. Iwamoto, K. Goto, H. Murakami, Y. Kumagai, N. Sarukura, M. Yoshimura, and M. Nakajima, "Anisotropic complex refractive index of β-Ga_2O_3 bulk and epilayer evaluated by terahertz time-domain spectroscopy," Applied Physics Letters **118**, 042101 (2021).
18. V. C. Agulto, T. Iwamoto, H. Kitahara, K. Toya, V. K. Mag-usara, M. Imanishi, Y. Mori, M. Yoshimura, M. Nakajima, "Terahertz time-domain ellipsometry with high precision for the evaluation of GaN crystals with carrier densities up to 10^{20} cm^{-3}" Scientific Reports **11**, 18129 (2021).
19. G. Fitzky, M. Nakajima, Y. Koike, A. Leitenstorfer, and T. Kurihara, "Ultrafast Control of Magnetic Anisotropy by Resonant Excitation of 4*f* Electrons and Phonons in $Sm_{0.7}Er_{0.3}FeO_3$" Physics Review Letters **127**, 107401 (2021).
20. M. A. Ordal, R. J. Bell, R. W. Alexander, L. L. Long, and M. R. Querry, "Optical properties of fourteen metals in the infrared and far infrared: Al, Co, Cu, Au, Fe, Pb, Mo, Ni, Pd, Pt, Ag, Ti, V, and W," Applied Optics **24**, 4493 (1985).
21. J. D. Kraus, "The Helical Antenna," in *Antennas*, 2nd ed. (McGraw-Hill, 1997), pp. 265–339.
22. Z. He, L. Wu, Y. Liu, Y. Lu, F. Wang, W. Shao, S. Fu, and G. Tong, "Ultrawide bandwidth and large-angle electromagnetic wave absorption based on triple-nested helix metamaterial absorbers," Journal of Applied Physics **127**, 174901 (2020).
23. T. Notake, T. Iyoda, T. Arikawa, K. Tanaka, C. Otani, and H. Minamide, "Dynamical visualization of anisotropic electromagnetic re-emissions from a single metal micro-helix at THz frequencies," Scientific Reports **11**, 3310 (2021).